CONTRIBUTION NO. 1445 FROM THE CENTRAL RESEARCH DEPARTMENT,
EXPERIMENTAL STATION, E. I. DU PONT DE NEMOURS AND COMPANY, WILMINGTON, DELAWARE 19898

Transition Metal Pyrite Dichalcogenides. High-Pressure Synthesis and Correlation of Properties

BY T. A. BITHER, R. J. BOUCHARD, W. H. CLOUD, P. C. DONOHUE, AND W. J. SIEMONS

Received April 17, 1968

The pyrite-type dichalcogenides ZnS_2, $ZnSe_2$, CdS_2, and $CdSe_2$ have been synthesized at high pressure (65–89 kbars). Electrical, magnetic, and spectral data have been obtained on the pyrite series of compounds MX_2 (many in single-crystal form) where M = Fe, Co, Ni, Cu, Zn and X = S, Se, Te (no $ZnTe_2$). These data have been used to develop a qualitative band model that allows a consistent interpretation of the diverse properties of the MnX_2 to ZnX_2 pyrite group of compounds. The importance of covalent interaction between the cation and the chalcogen is emphasized. This interaction leads to a broadening of the cation e_g levels into a band of collective antibonding electron states which can lead to metallic conductivity when partially filled. A new computer technique is described for evaluating the results of reflectance measurements made with polarized light.

Introduction

Transition metal dichalcogenides having the pyrite-type structure occur in the 3d series as the known mineral or synthetic compounds MnS_2 (hauerite), $MnSe_2$, $MnTe_2$, FeS_2 (pyrite), CoS_2, $CoSe_2$, NiS_2, and $NiSe_2$. The use of high-pressure syntheses to extend this range to include the compounds CuS_2, $CuSe_2$, $CuTe_2$, $NiTe_2$, $CoTe_2$, $FeSe_2$, and $FeTe_2$ has recently been reported by us.[1] The same technique has now been used to prepare the new $3d^{10}$ and $4d^{10}$ pyrite-type compounds ZnS_2, $ZnSe_2$, CdS_2, and $CdSe_2$ as well as a number of mixed cation[2] compositions with the same structure. The magnetic, electrical, and optical properties of these new materials have been examined as well as those of certain of the known pyrite compounds, which were prepared by vapor-transport and/or high-pressure techniques. These data combined with information from the literature have now been used to correlate the properties of this isotypic d^5–d^{10} series in terms of a simplified band picture.

Experimental Section

Preparation of Compounds.—High-pressure reactions were run at 60–65 kbars, unless otherwise indicated, in a tetrahedral anvil press of National Bureau of Standards design[3] using a cylindrical boron nitride crucible surrounded by a graphite-sleeve resistance heater inserted in a pyrophyllite tetrahedron. Temperature was measured with a Pt–Rh thermocouple, uncorrected for pressure effects, which was adjacent to the graphite heater. The operating procedure has been described elsewhere.[1] High-purity reactants ("four nines plus") were ground together and were pelleted prior to reaction. Depending on reactant densities, pellets weighed 0.1–0.7 g. This technique was used to prepare pyrites of the types MS_2 (M = Zn, Cd, Cu, Ni), MSe_2 (M = Zn, Cd, Cu, Ni, Co, Fe), and MTe_2 (M = Cu, Ni, Co, Fe). Variable parameters such as reactant ratios, temperature cycles, and pressures were found to depend on the compound being prepared and are detailed in the Results.

In addition, the disulfides of Fe, Co, and Ni, which normally adopt the pyrite-type crystal structure under ambient conditions, were prepared in single-crystal form in sealed silica tubes using either an iodine or a chlorine vapor transport technique.[4]

X-Ray Data.—Debye–Scherrer X-ray diffraction powder data were obtained at 25° on the reaction products. Patterns that showed the pyrite-type structure were indexed, and the unit-cell dimensions were refined by a least-squares method with the Nelson–Riley function[5] as one parameter. Cell dimensions are within a precision range of ±0.0005 Å in the cases where five significant figures are reported.

Electrical and Magnetic Measurements.—Except for ZnS_2 and CdS_2, electrical resistivity was measured on reasonably well-shaped single crystals using a four-probe technique described previously.[6] The disulfides of Zn and Cd were isolated as powders and resistivity was measured on compacts held at a pressure of about 40 tons/in.^{2}. Activation energy of resistivity, E_a, as reported herein is defined by the relation $\rho = \rho_0 e^{E_a/kT}$.

Hall constants were measured on single crystals of FeS_2 and CoS_2 and on a polycrystalline piece of CuS_2. An alternating electric field of 10 cps was applied, and the Hall voltage was detected with a lock-in amplifier. The magnetic field was 15,000 Oe or less. The Hall constants (Tables I and II) were independent of the magnetic field.

A vibrating sample magnetometer and/or a Faraday balance were used to measure magnetic properties. Measurements were first made on powders or polycrystalline chunks. When single crystals became available, their magnetic properties were found to agree with those of powder specimens. The measurements covered the temperature range 4.2–300°K except for CoS_2 and NiS_2 for which it was extended to 700 and 400°K, respectively. Saturation magnetizations were measured in fields up to 17,500 Oe, Curie temperatures in fields of 50–300 Oe, and susceptibilities in fields of 2000–17,500 Oe.

Optical Measurements.—Specular, near-normal-incidence, reflectance spectra were measured from 0.5 to 5.0 eV. The incident light was white and unpolarized. The reflected light was analyzed in a Perkin-Elmer 112 monochromator. The reflecting surfaces were as-grown crystal faces of FeS_2, CoS_2, and NiS_2 and polished surfaces of polycrystalline pieces of CuS_2, CuSSe, $CuSe_2$, CuSeTe, and $CuTe_2$. The optical constants were calculated from the observed spectra by a Kramers–Kronig calculation.[7] At the high-frequency side of the observation range, an extrapolation formula of Rimmen and Dexter[7,8] was used, while on the low-frequency side, for the metallic samples, reflectance values were used that had been calculated by an approximation

(1) T. A. Bither, C. T. Prewitt, J. L. Gillson, P. E. Bierstedt, R. B. Flippen, and H. S. Young, *Solid State Commun.*, **4**, 533 (1966).
(2) T. A. Bither and P. C. Donohue, to be submitted for publication.
(3) E. C. Lloyd, U. O. Hutton, and D. P. Johnson, *J. Res. Natl. Bur. Std.*, **C63**, 59 (1959).
(4) R. J. Bouchard, *J. Cryst. Growth*, **2**, 40 (1968).
(5) J. B. Nelson and D. P. Riley, *Proc. Phys. Soc.* (London), **57**, 160 (1945).
(6) T. A. Bither, J. L. Gillson, and H. S. Young, *Inorg. Chem.*, **5**, 1559 (1966).
(7) F. Stern, *Solid State Phys.*, **15**, 299 (1963).
(8) M. P. Rimmen and D. L. Dexter, *J. Appl. Phys.*, **31**, 775 (1960).

TABLE I

ZnX_2, CdX_2, AND CuX_2 PYRITES

Compound	a, Å	Resistivity at 25°, ohm cm	E_a, eV	Seebeck coefficient, μV/deg	Supercond critical temp range, °K	Susceptibility at 25° × 10^6, emu/g
ZnS_2	5.9542	1.0×10^6				−0.36
$ZnSe_2$	6.2930	2.0×10^6	0.24			
CdS_2	6.3032	3.0×10^5	0.23			−0.41
$CdSe_2$	6.615	[a]				
CuS_2	5.7898	1.5×10^{-4}	Metallic	+3 ($R_H = -1.9 \times 10^{-3}$ cm³/C)[b]	1.48–1.53	0.29
CuSSe	5.923	9.5×10^{-5}	Metallic	+3	1.5–2.0	
$CuSe_2$	6.1166	7.5×10^{-5}	Metallic	+2	2.30–2.43	0.42
CuSeTe	6.302	6.8×10^{-4}	Metallic		1.6–2.0	0.39
$CuTe_2$	6.6052	5.6×10^{-4}	Metallic	+8	1.25[c]–1.3	−0.40

[a] No data; $CdSe_2$ mixed with CdSe. [b] Hall constant at room temperature. [c] 1.25°K lowest temperature of measurement.

TABLE II

NiX_2, CoX_2, AND FeX_2 PYRITES

			Electrical data			Magnetic data
MX_2	Method of prepn[a]	a, Å	Resistivity at 25°, ohm cm	E_a, eV	Seebeck coefficient, μV/deg	
NiS_2	ST–P	5.6887[b]		0.25 (500°K)[c]		$\mu_{eff} = 3.2\ \mu_B$, $\theta = -1500$°K[d]
	HT–X ($NiS_{1.99}$)	5.6874	6×10^{-1}	0.12 (298°K) 0.32 (500°K)	+311	
	HP–65–X ($NiS_{2.01}$)	5.6761	5×10^{-3}	0.01 (298°K)	+9	$\mu_{eff} = 3.8\ \mu_B$,[e] $\theta = -1800$°K, $\chi_{298°K} = 6 \times 10^{-6}$ emu/g
$NiS_{1.6}Se_{0.4}$	ST–P			Zero[e]		
$NiSe_2$	ST–P[f] ($NiSe_{2.00}$)	5.9604		Metallic[c]		$\mu_{eff} = 1.34\ \mu_B$[f]
	HP–65–X ($NiSe_{2.01}$)	5.9573	1×10^{-4}	Metallic	−7	Wk temp-indep paramag, $\chi \simeq 1 \times 10^{-6}$ emu/g
$NiTe_2$	ST–P or HP–65–X	CdI_2 type		Metallic		
	HP–89–X (Pyrite + CdI_2)	6.374		Metallic, no T_S[h] to 1.3°K		
CoS_2	ST–P	5.528[i]		Metallic[c]		$\mu_{eff} = 1.85\ \mu_B$,[i] ferromag,[d] $\mu_S = 0.84\ \mu_B$, $T_C = 110$°K
	HT–X ($CoS_{1.99}$)	5.5359	2×10^{-4}	Metallic	−28 ($R_H = -1.1 \times 10^{-3}$ cm³/C)[l]	$\mu_{eff} = 1.84\ \mu_B$, $\theta = 193$°K, $\mu_S = 0.89\ \mu_B$, $T_C = 118$°K
$CoSe_2$	ST–P[k] ($CoSe_{2.00}$)	5.8588		Metallic[c]		$\mu_{eff} = 2.56\ \mu_B$,[g,k] $\chi_{293°K} = 4.6 \times 10^{-6}$ emu/g
	HP–65–X	5.8564	2×10^{-4}	Metallic	−23	$\mu_{eff} = 2.44\ \mu_B$,[g] $\theta = -455$°K, $\chi_{298°K} = 4.4 \times 10^{-6}$ emu/g
	HT–X	5.856	7×10^{-5}	Metallic		Wk temp-indep paramag, $\chi \simeq 6 \times 10^{-7}$ emu/g
$CoTe_2$	HP–65–X	6.3182	1×10^{-4}	Metallic, no T_S[h] to 1.3°K	−1	Wk temp-indep paramag, $\chi \simeq 2 \times 10^{-6}$ emu/g
FeS_2	HT–X ($FeS_{2.00}$)	5.4182	1.74	0.01 (<60°K) 0.20 (298°K) 0.46 (500°K) ($\Delta E_{opt} = 0.9 \pm 0.1$)	−500 ($R_H = -4.0 \times 10^2$ cm³/C)[l] ($\mu_e = 230$ cm²/V sec)[m]	$\mu_{eff} \simeq 0$
$FeSe_2$	HP–65–X ($FeSe_{1.95}$)	5.7859	2×10^{-2}	0.1 (298°K)	−28	$\mu_{eff} \simeq 0$
$FeTe_2$	HP–65–X	6.2937	2×10^{-3}	ρ–T curve flat, He → room temp	−25	$\mu_{eff} \simeq 0$

[a] ST–P, sealed tube–powder; HT–X, halogen transport–crystals; HP–n–X, high pressure–n kilobars–crystals. [b] R. J. Bouchard, *J. Cryst. Growth*, **2**, 40 (1968). [c] F. Hulliger, *Helv. Phys. Acta*, **32**, 615 (1959). [d] R. Benoit, *J. Chim. Phys.*, **52**, 119 (1955). [e] F. Hulliger, *J. Phys. Chem. Solids*, **26**, 639 (1965). [f] F. Grønvold and E. Jacobsen, *Acta Chem. Scand.*, **10**, 1440 (1956). [g] Corrected for core diamagnetism. [h] Superconducting transition. [i] A. F. Andresen, S. Furuseth, and A. Kjekshus, *Acta Chem. Scand.*, **21**, 833 (1967). [j] L. Néel and R. Benoit, *Compt. Rend.*, **237**, 444 (1953). [k] F. Bøhm, F. Grønvold, H. Haraldsen, and H. Prydz, *Acta Chem. Scand.*, **9**, 1510 (1955). [l] Hall constant at room temperature. [m] Hall mobility.

formula derived by Hagen and Rubens[9] for the reflectivity of metals in the infrared region. Iron disulfide and NiS_2, the only nonmetallic samples, were assumed to be transparent. The correctness of these extrapolations was checked by comparison of the calculated values of the optical constants with those obtained from direct measurements at 2.29 and 3.03 eV. The experimental results are reported in the form of n and k, the real and imaginary parts of the complex refractive index $\tilde{n} = n + ik$,

(9) E. Hagen and H. Rubens, *Ann. Physik*, **11**, 873 (1903). See M. Burn and E. Wolf, "Principles of Optics," 3rd ed, Pergamon Press Ltd., London, 1965, p 622.

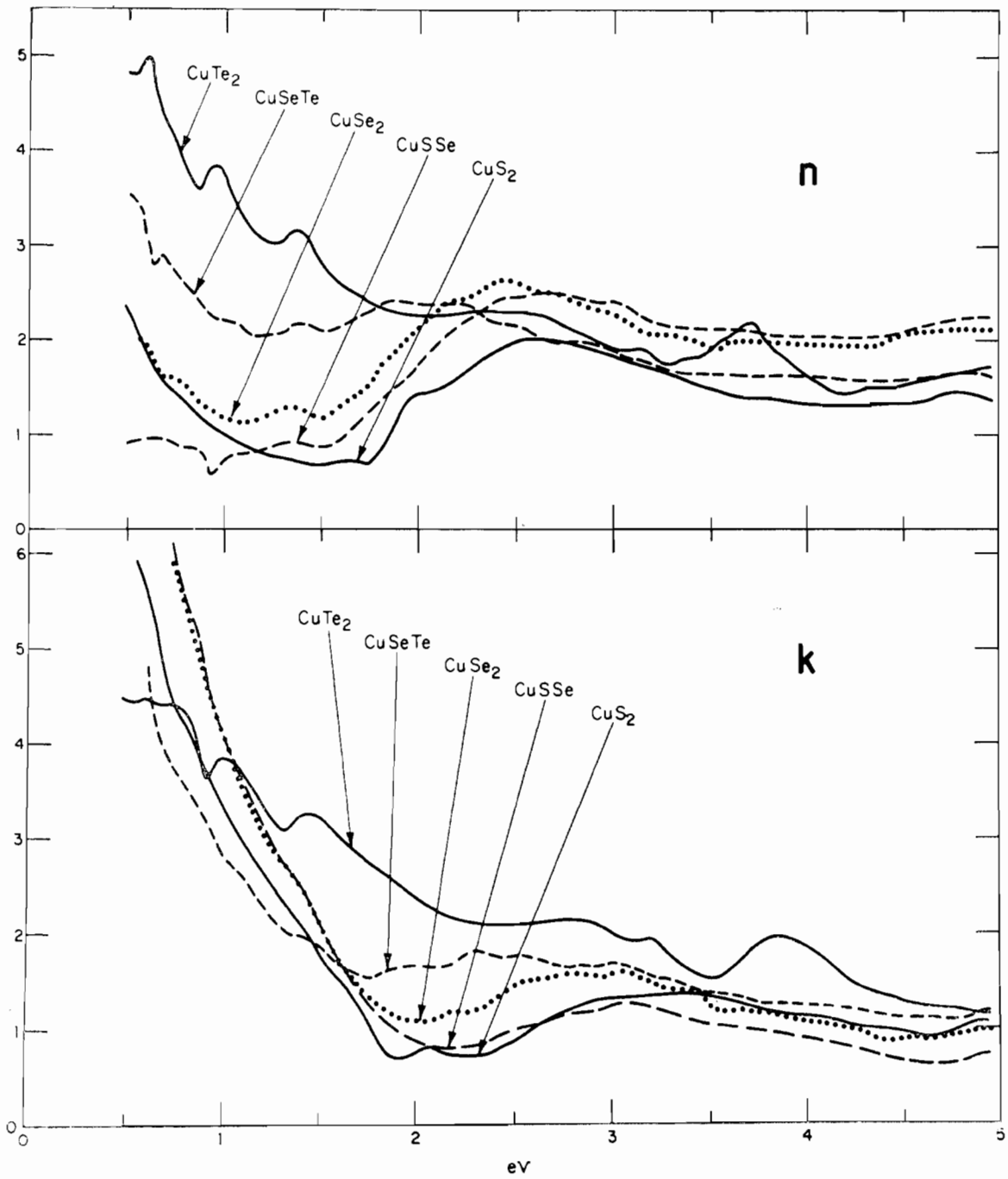

Figure 1.—Real and imaginary parts of the complex refractive index for CuX_2 dichalcogenides.

as calculated from the Kramers–Kronig relations (Figures 1 and 2). The absorption constant α is equal to $4\pi k/\lambda$.

Direct measurements of the optical constants were made by determining the ratio $\rho^2(\theta) = R_\parallel(\theta)/R_\perp(\theta)$ as a function of the angle of incidence θ, where $R_\parallel$ and $R_\perp$ are the reflectivities for light polarized, respectively, parallel and perpendicular to the plane of incidence. This technique has been described by Avery.[10] Since the optical constants cannot be expressed explicitly as functions of $\rho^2(\theta)$, Avery made measurements at selected values of θ and used specific graphs for each of these values of θ. A mapping procedure has also been described for the evaluation of measurements at two values of θ.[11]

For each sample, ρ^2 was determined at approximately ten values of θ in this work. In the neighborhood of the Brewster angle, measurements were made at 2.5° intervals and elsewhere at 5° intervals. An iterative computer-search program[12] was used for finding the values of the optical constants that gave the best-fitting calculated curve of $\rho^2(\theta)$ *vs.* θ throughout the observations. In all cases, differences between observed and calculated values of ρ^2 were within the experimental accuracy.

In order to facilitate the interpretation of the optical measurements, the integral $\int_0^{\omega_0}\omega \mathrm{Im}\tilde{\epsilon}(\omega)\,d\omega$ was calculated for all samples, where $\mathrm{Im}\tilde{\epsilon}(\omega)$ is the imaginary part of the complex dielectric constant $\tilde{\epsilon}(\omega)$. The relation with the optical constants is $\mathrm{Im}\tilde{\epsilon}(\omega) = 2nk$. For FeS_2, the integral $\int_0^{\omega_0}\omega^{-1}\mathrm{Im}\tilde{\epsilon}(\omega)\,d\omega$ was also calculated (Figures 3 and 4).

Results

ZnX_2 and CdX_2.—Pyrite-type ZnS_2 mixed with some unreacted starting materials was obtained as a bright

(10) G. Avery, *Proc. Phys. Soc.* (London), **B64**, 1087 (1951); **B65**, 425 (1952).

(11) R. E. Lindquist and A. W. Ewald, *J. Opt. Soc. Am.*, **53**, 247 (1963).

(12) The program was written by J. P. Chandler of Indiana University and is available as Program No. 66.1 through the Quantum Chemistry Program Exchange, Indiana University, Bloomington, Ind. 47401.

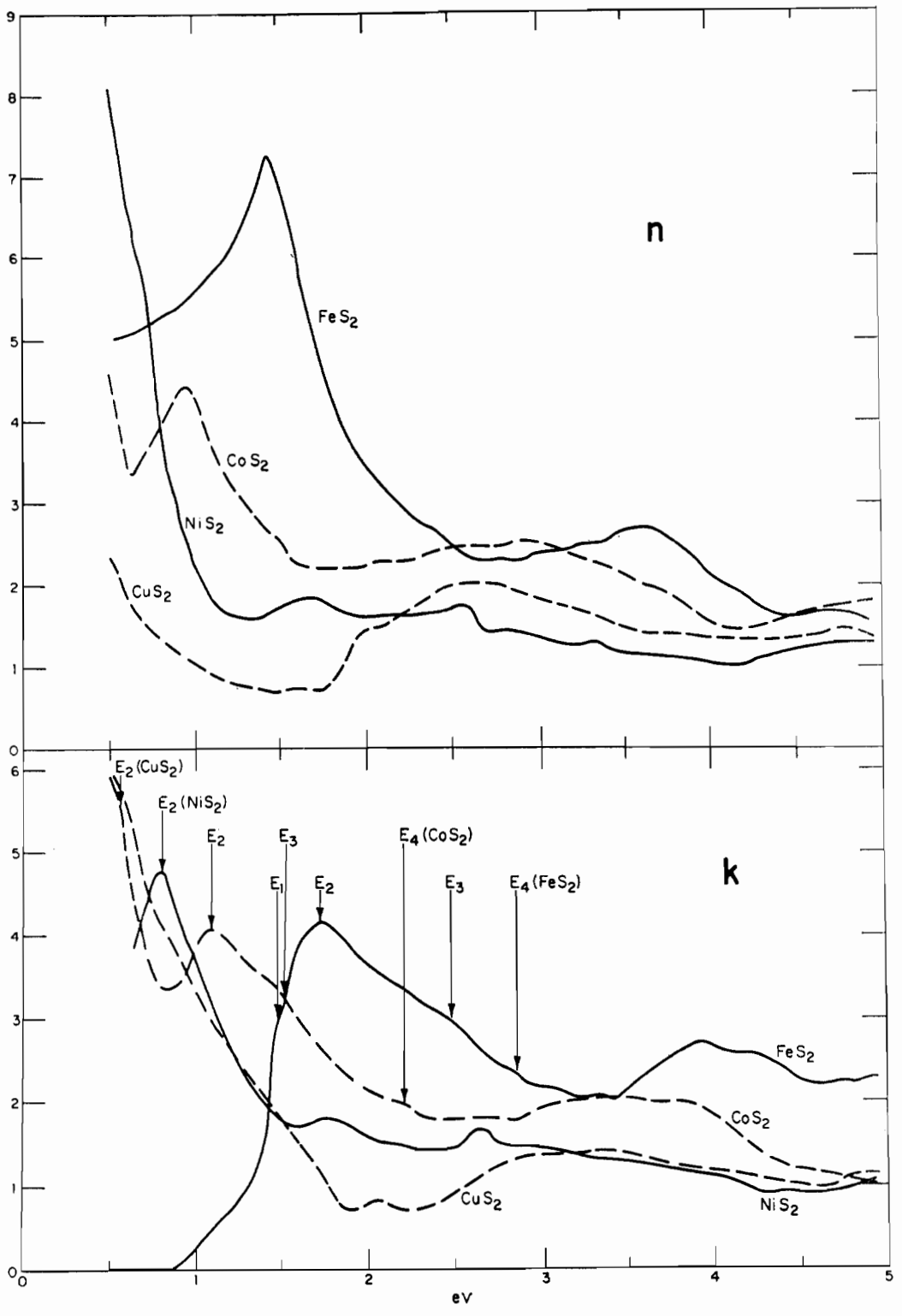

Figure 2.—Real and imaginary parts of the complex refractive index for FeS_2, CoS_2, NiS_2, and CuS_2.

yellow, microcrystalline powder by reaction of ZnS + S at 65 kbars for 4–6 hr at 400–600° followed by a rapid quench to room temperature. The thermal stability limit of about 600° at 65 kbars could be raised to 1200° by use of 89 kbars of pressure. In an attempt to improve both the ZnS_2 crystallite size and the yield, an essentially amorphous zinc polysulfide prepared according to the method of Grillot[13] was treated with variable amounts of sulfur at 65 kbars of pressure. A small amount of unreacted ZnS and a high-pressure form of sulfur[14] were frequently obtained, and the ZnS_2 remained microcrystalline. X-Ray diffraction powder patterns of all ZnS_2 compositions prepared showed the pyrite-type structure having the same unit cell size with $a = 5.9542$ Å. Zinc analysis on one product showing no ZnS or S in its X-ray diffraction pattern indicated

(13) E. Grillot, *Bull. Soc. Chim. France*, 39 (1951).

(14) S. Geller, *Science*, **152**, 644 (1966).

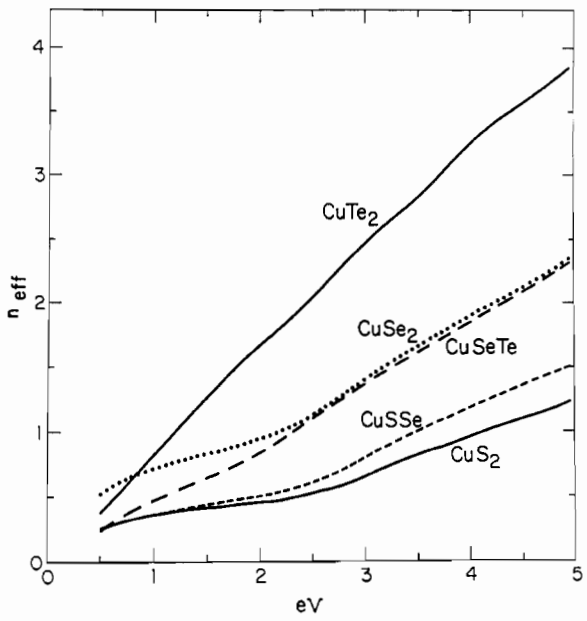

Figure 3.—Number of electrons, n_{eff}, participating in optical transitions of the CuX_2 dichalcogenides.

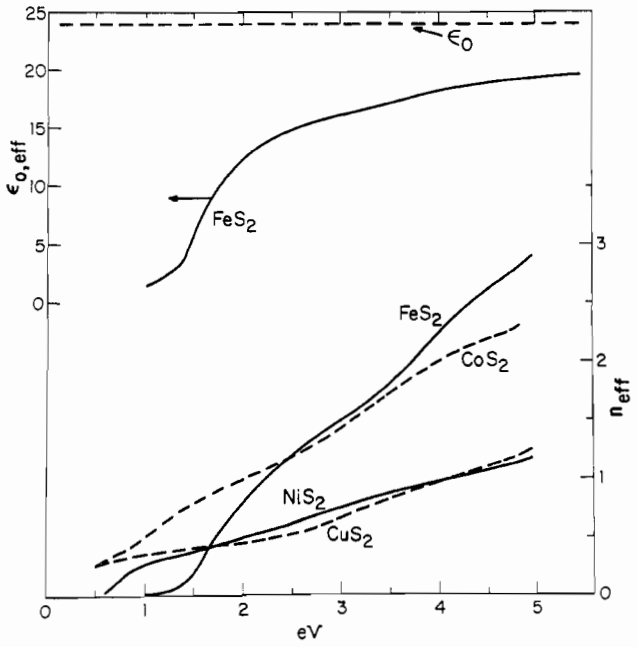

Figure 4.—Number of electrons, n_{eff}, participating in optical transitions of FeS_2, CoS_2, NiS_2, and CuS_2.

essentially ZnS_2 stoichiometry. *Anal.* Calcd for ZnS_2: Zn, 50.48. Found: Zn, 50.36. X-Ray examination of ZnS_2 at elevated temperature showed it to be stable at 200° in a sealed, evacuated capillary but to be decomposed to ZnS at 250°.

Pyrite-type CdS_2, as a microcrystalline yellow-brown powder, was formed from either CdS or amorphous cadmium polysulfide[13] and S in the same manner and under the same conditions used to prepare ZnS_2. Powders resulted and all X-ray diffraction patterns showing the pyrite-type structure again had the same unit cell size with $a = 6.3032$ Å, suggesting a uniform Cd to S stoichiometry. Thermogravimetric analysis under argon on one sample indicated a compound $CdS_{1.94}$ decomposing to CdS over the temperature range 200–300° at atmospheric pressure. Assuming the formula CdS_2, the presence of about 6% CdS impurity accounts for the stoichiometry obtained. In confirmation, a Debye–Scherrer X-ray pattern suggested a trace of CdS in this material.

Zinc diselenide was prepared by reaction of Zn + 2.5Se at 65 kbars for 1 hr at 600–800°, a 4–5 hr slow cool to 500°, and a subsequent quench to room temperature. Well-formed crystals with a metallic appearance could be isolated from the ends of these reaction products but in the center the same material was mixed with Se plus yellow-brown ZnSe. X-Ray diffraction powder data showed the crystals to have the pyrite-type structure with cell dimension $a = 6.2930$ Å.

Two series of reactions of Cd + 2Se yielding pyrite-type cadmium diselenide were carried out at 65 kbars: (1) a 3–6-hr heating at 600° followed by either a direct quench or a 3-hr cool to 300° before quenching; (2) a 0.5-hr heating at 800° followed by a 0.5-hr cool to 400–500° and a 5-hr hold in this temperature range prior to quenching. Reactions quenched from temperatures higher than 600° failed to give a pyrite phase. In contrast to $ZnSe_2$, a single-phase $CdSe_2$ material was not isolated for characterization. Crystals of CdSe usually formed at the ends of the reaction crucible accompanied by an intimate mixture of $CdSe_2$, CdSe, and Se in the center of the boule. X-Ray diffraction powder data on this mixture indicated a pyrite-type phase with cell dimension $a = 6.615$ Å.

The reaction of Zn + 2Te at 65 kbars for 2 hr at 1200° followed by a 4-hr cool to 400° and a subsequent quench gave a heterogeneous mixture of ZnTe at the sample ends, Te in the center, and a mixture of red ZnTe plus small silvery platelets between. The silver-like phase could not be isolated for characterization, but X-ray powder data thereon were indexed on the basis of a hexagonal unit cell with $a = 3.98$ and $c = 5.25$ Å, suggesting formation of a CdI_2-type $ZnTe_2$ phase.

These compounds containing zinc and cadmium, with their filled 3d and 4d shells, showed the expected diamagnetism and semiconductor behavior in the cases where measurements were carried out (Table I). The activation energies of resistivity are relatively low, but, from the yellow color of both ZnS_2 and CdS_2, a band gap of at least 2.5 eV is estimated which is presumed to correspond to the excitation of an electron from the filled d level up to the appropriate higher sp antibonding level. It was not possible to obtain unequivocal values of the energy gaps of these compounds from optical measurements because diffuse scattering by the finely particulate material interfered with the observation of the absorption edge.

CuX_2.—Conditions for the high-pressure synthesis at 65 kbars of the pyrite-type compounds CuS_2, $CuSe_2$, and $CuTe_2$ as well as the mixed anion compositions CuSSe and CuSeTe have been reported by us.[1] Additional synthesis studies carried out on a CuS–S mixture by quenching from selected P–T conditions indicate a

wide region of thermal stability for CuS_2 in the pressure range 15–65 kbars; *i.e.*, CuS_2 was formed from 15 kbars (400°) to 65 kbars (400–1600°).

These copper dichalcogenides all show metallic conductivity (for CuS_2, see Figure 5) coupled with weak, temperature-independent magnetic susceptibility. They also show superconductivity with a maximum critical temperature of 2.4°K for the composition $CuSe_2$ (Table I). Munson, *et al.*,[15] reported a small localized moment, $\mu_{eff}^2 = 0.34\,\mu_B^2$, to be present in CuS_2. This observation is not in agreement with our measurements on the same compound and is incompatible with the observed superconductivity. The presence of a second impurity phase is suggested as the source of this moment.

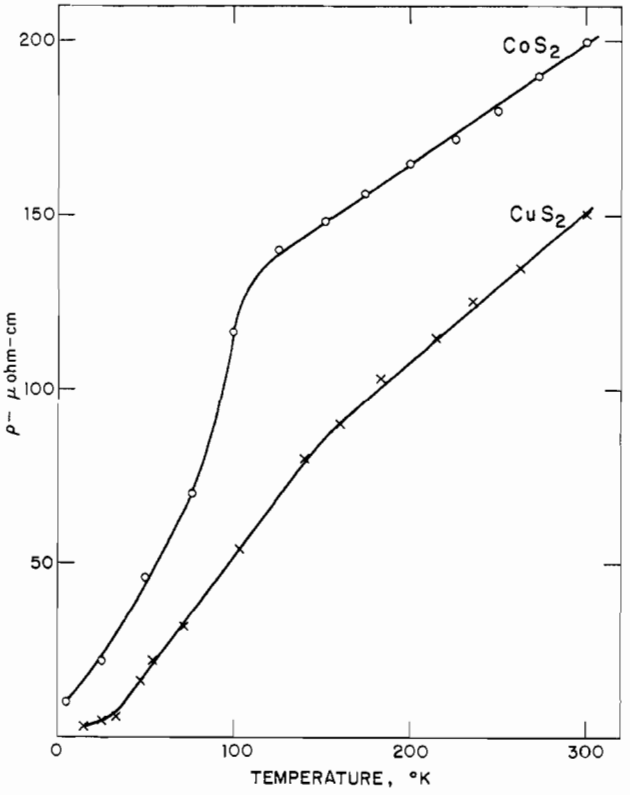

Figure 5.—Resistivity of CuS_2 and CoS_2.

Since small, positive Seebeck voltages were also observed for these compositions, hole conductivity is suggested. The Hall constant, however, was found to be -1.9×10^{-3} cm³/C for CuS_2 which corresponds to 0.16 carrier per molecule. Room-temperature values of the real and imaginary parts of the complex refractive index in the range 0.5–5.0 eV are shown in Figure 1 for all of the copper compounds. The values for CuS_2 are also shown in Figure 2.

NiX_2.—At atmospheric pressure, both nickel disulfide and diselenide readily form in the pyrite structure. Electrical and magnetic studies on NiS_2[16–18] and $NiSe_2$[17,19] have been reported. From resistivity measurements made on a compacted powder of NiS_2, Hulliger[16] observed semiconductor behavior with an activation energy of resistivity of about 0.25 eV. From susceptibility measurements, Benoit[18] indicated a Curie–Weiss type of behavior for NiS_2 with a μ_{eff} of 3.19 μ_B coupled with an extremely large negative θ of about −1500°K. In contrast, $NiSe_2$ was found[16] to have metallic conductivity, and Grønvold and Jacobsen[19] reported a non-Curie–Weiss type of behavior involving a very weak magnetic susceptibility that increased from 0.66×10^{-6} emu/g at liquid N_2 temperature to 0.90×10^{-6} emu/g at 450°. Hulliger[17] examined the mixed anion compositions $NiS_{2-x}Se_x$ and noted that the energy gap decreased with increasing Se content, going to zero near $x = 0.4$.

Single crystals of pyrite-type nickel disulfide were prepared in this work for comparative studies by both a halogen-transport technique[4] and a synthesis under high pressure in the anvil. For the latter, reaction of either NiS + S or Ni + 2.3S at 65 kbars for 2 hr at 1200°, a 4-hr cool to 400°, and a subsequent quench to room temperature gave shiny black crystals, some of which approached 1 mm in size. Crystals up to 2–3 mm on an edge could be obtained by chlorine transport. These crystals were analyzed by thermogravimetry with the weight loss being measured both after oxidation and after subsequent reduction to nickel metal. Crystals prepared in the tetrahedral anvil press were found to contain a very slight excess of sulfur. *Anal.* Calcd for NiS_2: S, 52.21. Found: S, 52.3. However, those made by halogen transport were slightly sulfur deficient. *Anal.* Calcd for NiS_2: S, 52.21. Found: S, 52.1. The latter were also found to contain 89 ppm of chlorine by neutron activation analysis. It should be emphasized that these deviations from stoichiometry, while consistent and reproducible, are within experimental error.

Halogen-transported NiS_2 showed semiconductor behavior with an activation energy of 0.32 eV above room temperature and a Seebeck voltage of +311 μV/deg. In contrast, samples prepared at high pressure showed a nearly temperature-independent resistivity some two decades lower than that of the halogen-transported material, coupled with a low Seebeck voltage of +9 μV/deg. Since the resistivity and activation energy are markedly greater for the chlorine-transported single crystals, it is assumed that their behavior is much closer to that of intrinsic material. The variation in activation energy with temperature of these same crystals, however, may be due to the incorporation of halogen. Thus, the smaller low-temperature activation energy may result from the presence of halogen-doping levels providing electrons for conductivity. Although the samples prepared at high pressure were also stoichiometric within experimental error, they consistently exhibited extrinsic behavior at low temperatures. Sample decomposition precluded further measurements at higher tempera-

(15) R. A. Munson, W. DeSorbo, and J. S. Kouvel, *J. Chem. Phys.*, **47**, 1769 (1967).
(16) F. Hulliger, *Helv. Phys. Acta*, **32**, 615 (1959).
(17) F. Hulliger, *J. Phys. Chem. Solids*, **26**, 639 (1965).
(18) R. Benoit, *J. Chim. Phys.*, **52**, 119 (1955).
(19) F. Grønvold and E. Jacobsen, *Acta Chem. Scand.*, **10**, 1440 (1956).

tures. These electrical data are summarized in Table II and Figure 6.

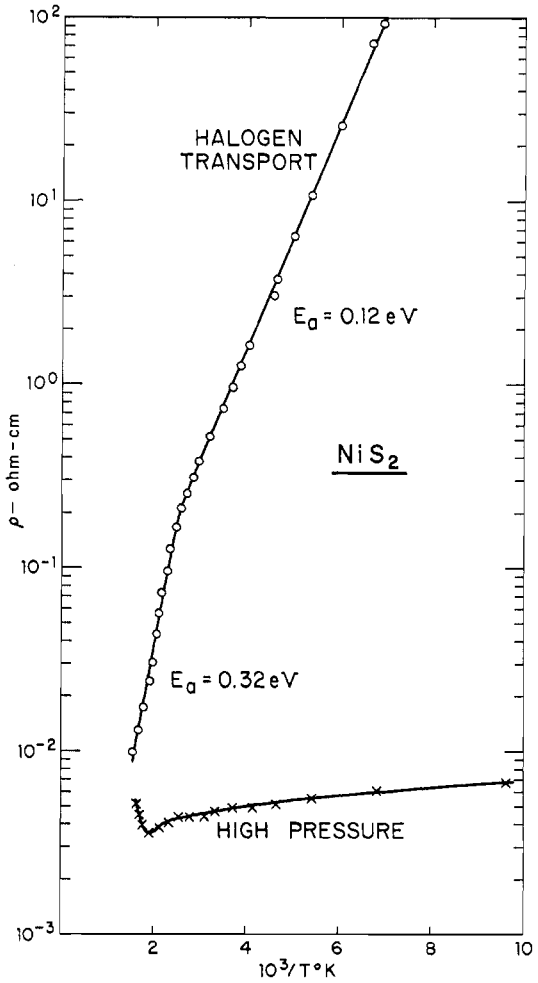

Figure 6.—Resistivity of NiS_2.

Nickel disulfide samples prepared at both low and high pressure showed essentially the same magnetic susceptibility behavior except at very low temperatures. Field-independent values of 6×10^{-6} and 7×10^{-6} emu/g were observed at 300 and 77°K, respectively. Within experimental error, a plot of the reciprocal susceptibility *vs.* temperature gave a straight line with a very large negative intercept, -1800 ± 200°K, and a slope corresponding to $\mu_{eff}^2 \simeq 14\ \mu_B^2$. The data are in essential agreement with those of Benoit.[18] At 4.2°K, low-pressure, semiconducting NiS_2 prepared in either powder or single-crystal form showed weak ferromagnetism, $\mu_S = 0.02\ \mu_B$, with a Curie temperature of approximately 30°K. In contrast, high-pressure, metallic NiS_2 did not show this low-temperature ferromagnetism.

The low-temperature ferromagnetic moment appears to be related to the sulfur deficiency observed in NiS_2 formed at low pressure. If this material is heated with excess sulfur at 65 kbars (1200°), it no longer has a low-temperature moment. Under the same conditions without the excess sulfur, it still retains 75% of its low-temperature moment. The low value of the moment suggests that it originates in some deviation in stoichiometry from NiS_2. If, for example, the moments of Ni^+ resulting from sulfur deficiency ordered ferromagnetically, a 0.7% sulfur deficiency would account for the observed moment.

The large negative value for the Weiss constant, $\theta = -1800$°K, suggests antiferromagnetic ordering with a high Néel temperature. No peak in the susceptibility *vs.* temperature curve indicative of a Néel point is observed up to 400°K. Neutron diffraction shows no superstructure lines indicative of antiferromagnetic ordering down to 100°K.[20] The magnetic susceptibility of NiS_2 is so small and varies so slowly with temperature that the fit to a Curie–Weiss plot with a large negative intercept may be fortuitous. At the present time, it cannot be stated conclusively that there is a local moment on the nickel ion.

Room-temperature values of the real and imaginary parts of the complex refractive index for NiS_2 are shown in Figure 2.

Pyrite-type nickel diselenide in single-crystal form was also prepared at 65 kbars from Ni + 2Se under the same conditions as was NiS_2. The silvery, metallic-appearing crystals were analyzed by thermogravimetry. Like $NiS_{2.01}$ prepared in the anvil, a selenium-rich selenide, $NiSe_{2.01}$, was suggested from the analysis. *Anal.* Calcd for $NiSe_2$: Se, 72.90. Found: Se, 73.0.

Resistivity and Seebeck voltage measurements indicated metallic-type conduction for this material in agreement with the data of Hulliger.[16] Magnetic susceptibility data showed weak, temperature-independent paramagnetism. These data, indicating the presence of collective d electrons, are given in Table II.

Although NiS_2 and $NiSe_2$ form in the pyrite structure at atmospheric pressure, $NiTe_2$ occurs as the CdI_2 type. Reactions of Ni + 2Te at 65 kbars for 2 hr at 800–1200° followed by a 4-hr cool to 400° and a quench still gave CdI_2-type products. With an increase in pressure to 89 kbars, a 2-hr reaction at 1000° followed by a quench gave a product comprising both pyrite- and CdI_2-type nickel ditelluride that showed metallic-type behavior (Table II). Superconductivity was not observed down to 1.3°K. Collective d electrons are again suggested as with the diselenide.

CoX_2.—At atmospheric pressure, both cobalt disulfide and cobalt diselenide form in the pyrite structure while cobalt ditelluride occurs in two forms, either the marcasite or CdI_2 type, depending upon both the reaction temperature and the stoichiometry.[21]

Cobalt disulfide, which is a metallic conductor,[16] is unusual among these binary transition metal dichalcogenides in that it orders ferromagnetically at low temperature. Magnetic measurements on CoS_2, as reported by numerous workers, were discussed by Andresen, Furuseth, and Kjekshus[22] in their neutron diffraction study on this compound. All of these data on CoS_2 were obtained on powder samples. Single crys-

(20) S. Spooner, private communication.
(21) L. D. Dudkin and K. A. Dyul'dina, *Russ. J. Inorg. Chem.*, **4**, 1056 (1959).
(22) A. F. Andresen, S. Furuseth, and A. Kjekshus, *Acta Chem. Scand.*, **21**, 833 (1967).

tals were accordingly prepared for study by chlorine transport.[4] Sulfur-deficient material was obtained. *Anal.* Calcd for CoS_2: S, 52.11. Found: S, 52.0. The magnetic properties of this metallic conductor, which are compared with earlier results by Néel and Benoit[23] (Table II), show the same μ_{eff} but a slightly higher μ_S and Curie temperature. Results on this $CoS_{1.99}$ material are in agreement with recent measurements reported by Morris, Johnson, and Wold[24] on a similar $CoS_{1.97}$ phase. The resistivity *vs.* temperature curve for a single crystal of CoS_2 (Figure 5) shows a change in slope at the Curie temperature typical of ferromagnetic metals.[25]

The Hall data for CoS_2 correspond to considerably less than 1 e^- per molecule, *i.e.*, 0.24. While discrepancies between the number of electrons indicated from magnetic data and the number of electrons calculated from Hall data are not uncommon, it does suggest that the Fermi surface for the metallic pyrites is not a simple spherical one. This effect will become more pronounced as the number of electrons in the e_g band increases. As previously indicated for CuS_2, the Hall data correspond to only 0.16 carrier per molecule.

Room-temperature values of the real and imaginary parts of the complex refractive index for CoS_2 are shown in Figure 2.

Cobalt diselenide, which is also a metallic conductor,[16] is reported by Bøhm, *et al.*,[26] to show Curie–Weiss behavior to 90°K. Values of magnetic susceptibility were small, but a μ_{eff} of 2.56 μ_B was derived from their data.

For comparative purposes, single crystals of pyrite-type cobalt diselenide were prepared by reaction of Co + 2Se at 65 kbars under the same conditions as was NiS_2. Resistivity measurements and a low negative Seebeck voltage indicated metallic-type conduction (Table II). Magnetic susceptibility measurements from 300 to 4.2°K duplicated those of Bøhm, *et al.*,[26] to their termination point of 90°K (Table II).

Although a plot of susceptibility *vs.* temperature does not show a clear-cut Néel point, the curve of the inverse susceptibility *vs.* temperature departs from Curie–Weiss behavior at 55°K. The general shape of this curve is similar to that for $MnSe_2$ which was found by neutron diffraction studies[27] to be antiferromagnetic at liquid He temperature. Single crystals of $CoSe_2$ prepared by chlorine transport, however, showed weak temperature-independent paramagnetism (Table II).

Pyrite-type cobalt ditelluride was prepared by reaction of Co + 2Te at 65 kbars in the manner of NiS_2. The silvery, metallic-appearing product was observed to contain a minor amount of CdI_2-type phase as impurity. Resistivity measurements and a very low negative Seebeck voltage indicated metallic-type conduction as with CoS_2 and $CoSe_2$. No superconducting transition was observed down to 1.3°K. Magnetic susceptibility measurements showed very weak, almost temperature-independent paramagnetism from 4.2 to 300°K. These data, which are indicative of the presence of collective d electrons, are summarized in Table II.

FeX_2.—Iron disulfide occurs naturally both as the mineral pyrite, the structure prototype of this series of compounds, and as the orthorhombic mineral marcasite. The pyrite form of FeS_2 is obtained in laboratory syntheses except when unusual preparative conditions[28] are employed. In contrast, both $FeSe_2$ and $FeTe_2$, which also occur naturally, adopt the marcasite structure under ambient conditions.[29,30] Electrical measurements[31] on natural samples of pyrite-type FeS_2 indicated semiconductor behavior accompanied by wide variations in resistivity as well as magnitude of the Seebeck voltage. Depending upon the sample, either p- or n-type conduction was observed. Hall mobilities were 100 cm^2/V sec or less.[31] Magnetic measurements[18] indicated essentially diamagnetic behavior. The marcasite forms of $FeSe_2$ and $FeTe_2$ were reported by Fischer[29] and by Dudkin[30] to be semiconductors.

Single crystals of FeS_2 were prepared by chlorine transport.[4] *Anal.* Calcd for FeS_2: S, 53.45. Found: S, 53.4. They were n-type semiconductors (Table II) and exhibited a high Hall mobility (230 cm^2/V sec). The energy of activation at room temperature was relatively low (0.20 eV). At elevated temperatures a value of 0.46 eV was obtained (Figure 7) on a single crystal grown by iodine transport. This is in good agreement with absorption spectral measurements on the same material, which indicated an optical band gap of 0.9 ± 0.1 eV.

Room-temperature values of the real and imaginary parts of the complex refractive index for FeS_2 are shown in Figure 2.

Both iron diselenide and iron ditelluride were prepared as silvery crystals having the pyrite structure by reaction of Fe + 2Se or Fe + 2Te at 65 kbars for 2 hr at 1200°, a 4-hr cool to 400°, and a quench to room temperature. In the selenide system, Fe_3Se_4 formed at the ends of the sample container adjoined by selenium-deficient crystals of the pyrite phase. *Anal.* Calcd for $FeSe_{1.95}$: Se, 73.38. Found: Se, 73.4. Unreacted selenium was transported to the center. In contrast, in the Te system crystals of iron ditelluride formed at the sample ends. Calcd density for $FeTe_2$ with a = 6.2937 Å: 8.286 g/cm^3. Found: 8.223 g/cm^3. A deviation from $FeTe_2$ stoichiometry is indicated.

Pyrite-type $FeSe_2$ was a semiconductor like its marcasite counterpart (Table II). The resistivity of the ditelluride showed no change from liquid helium to room temperature. Magnetic susceptibility measurements indicated μ_{eff} of all three pyrite-type iron dichalcogenides to be essentially zero. The results of the magnetic

(23) L. Néel and R. Benoit, *Compt. Rend.*, **237**, 444 (1953).
(24) B. Morris, V. Johnson, and A. Wold, *J. Phys. Solids Chem.*, **28**, 1565 (1967).
(25) R. M. Bozorth, "Ferromagnetism," D. Van Nostrand Co., New York, N. Y., 1951, pp 763, 768.
(26) F. Bøhm, F. Grønvold, H. Haraldsen, and H. Prydz, *Acta Chem. Scand.*, **9**, 1510 (1955).
(27) J. M. Hastings, N. Elliott, and L. M. Corliss, *Phys. Rev.*, **115**, 13 (1959).
(28) G. Kullerud, Carnegie Institution of Washington Year Book, 1965–1966, p 352.
(29) G. Fischer, *Can. J. Phys.*, **36**, 1435 (1958).
(30) L. D. Dudkin and V. I. Vaidanich, *Sov. Phys. Solid State*, **2**, 1384 (1961).
(31) J. C. Marinace, *Phys. Rev.*, **96**, 593 (1954).

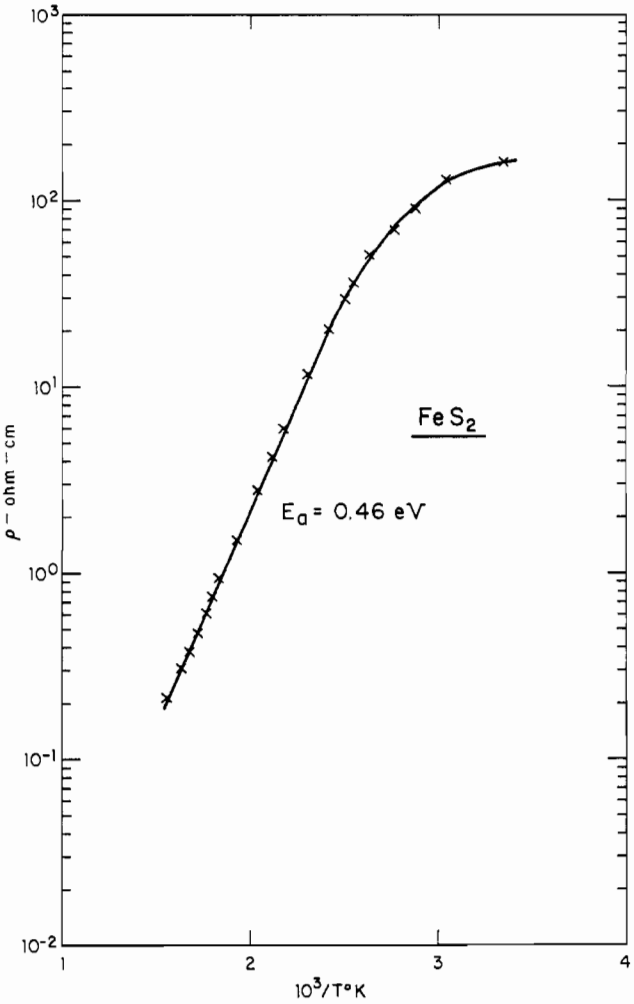

Figure 7.—Resistivity of FeS_2.

data were confirmed by Mössbauer measurements in which no magnetic ordering was observed for these pyrite-type iron dichalcogenides. These latter results were in agreement with Mössbauer measurements[32] on the three marcasite-type iron dichalcogenides.

Discussion

From the experimental results summarized herein, it is concluded that a band model is necessary to explain the properties of compounds with the pyrite structure. This conclusion is illustrated most strikingly by the following observations. FeS_2 is a high-mobility, diamagnetic semiconductor; CoS_2 is ferromagnetic and metallic; CuS_2 exhibits temperature-independent paramagnetism and is superconducting. For conciseness, this discussion will be concerned primarily with the sulfide series MS_2, where M = Mn, Fe, Co, Ni, Cu, and Zn. The only change occurring in this series is the progressive addition of d electrons. No other levels are affected. For this reason a simple qualitative band model should be sufficient to correlate the observed properties with a minimum of assumptions and approximations. In this series, MnS_2 is a special case and it actually may be more appropriately described by crystal field theory because of the very narrow bands expected. The reasons for this will be detailed later.

The fact that some of these materials have metallic properties forces consideration of the possible mechanisms by which delocalization of electrons can occur. Although metal–metal interactions can result in a band of available electron states, this does not seem to be an important consideration for these materials since the metal ions are too far apart (~4 Å) for sufficient overlap. This conclusion is based on empirical estimates[33] derived from the study of similar materials.

There is an alternate mechanism to explain metallic conductivity. The e_g orbitals of the metal ions, which point toward the near-neighbor anions, can form band states *via* covalent mixing of anion and cation wave functions.[34] This mixing is proportional to the anion polarizability and will increase in the series S → Se → Te. If the resulting band states are partially filled, metallic conductivity will result. The importance of covalency effects in this structure is exemplified by the fact that FeS_2 is diamagnetic, indicating low-spin Fe^{2+}, in contrast to the high-spin state observed in oxides. To discuss the energy level diagrams for the pyrites, it is necessary to know the coordination of the anions and the cations in the structure, which is described by Wells,[35] for example.

The anions occur in S_2 units, the center of the S–S bond being on alternate points of an NaCl-type lattice. The remaining lattice points are occupied by the cations. Each cation is surrounded by six anions in an octahedron compressed along the trigonal axis. Each sulfur atom is coordinated to three metal ions and another sulfur (the other half of the S–S unit) at the corners of a tetrahedron. Because of this coordination, it is assumed that the anions use hybridized sp^3 orbitals.

For the cation, the familiar octahedral crystal field energy level diagram is modified in two ways. There will be a major contribution to $10Dq$ from covalent bonding. In addition, because of the trigonal distortion, the t_{2g} orbitals will no longer be degenerate. For bonding to the anions, the cations will use orbitals that can be approximately described as $(e_g)^2sp^3$ hybrids. Bonding of σ type utilizing e_g orbitals will be considerably stronger than any π type (t_{2g}) because σ-orbital overlap is greater than π-orbital overlap. In this discussion, it is therefore assumed that the t_{2g} levels of the cation can be described as essentially nonbonding and can be treated as closed-shell core orbitals.

These considerations can be summarized in a general one-electron, one-molecule energy level diagram (Figure 8). The crystalline levels of the cation and anion are shown at the extreme left and extreme right of the diagram, respectively. The molecular orbitals formed by mixing anion and cation orbitals of proper symmetry are represented in the center of the diagram. The bonding electrons belong primarily to the anions, and the anti-

(32) A. A. Temperley and H. W. LeFevre, *J. Phys. Chem. Solids*, **27**, 85 (1966).

(33) J. B. Goodenough, "Magnetism and the Chemical Bond," Interscience Publishers, New York, N. Y., 1963, p 266.

(34) J. B. Goodenough, *Bull. Soc. Chim. France*, 1200 (1965).

(35) A. F. Wells, "Structural Inorganic Chemistry," 3rd ed, Oxford University Press, London, 1962, p 520.

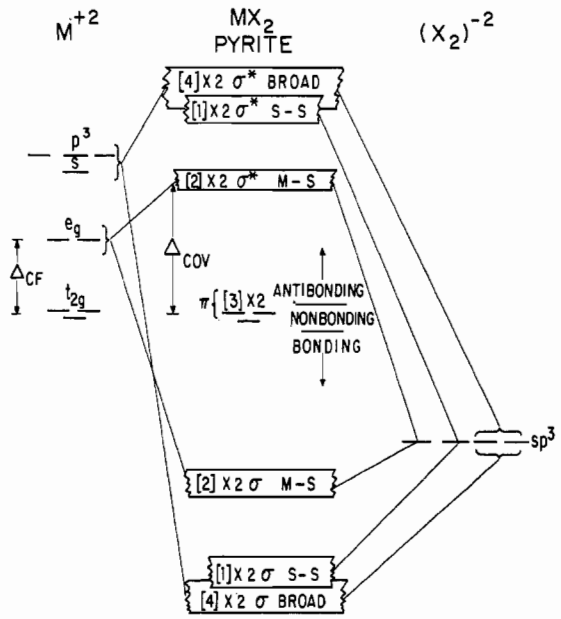

Figure 8.—Schematic one-electron, one-molecule energy level diagram for transition metal pyrites. The orbital degeneracy of each level is given in brackets and is multiplied by 2 because of spin degeneracy. Intraatomic exchange is ignored.

bonding electrons, primarily to the cations. Because of the higher electronegativity of the anions, they are lower on an energy level diagram than the cations. The covalent mixing of cation e_g and anion orbitals results in narrow bonding (σ) and antibonding (σ^*) bands. It should be noted that Δ_{cov} represents the difference between the strength of σ and π bonding, not the point charge interactions of crystal field theory.

It can be seen from the diagram that for the transition metal pyrites the bonding bands will always be filled (there are 14 electrons in the S_2^{2-} unit), and the highest antibonding band will always be empty. Therefore, only those states which originate from the transition metal d levels need be considered, and only these will be examined in the individual compounds. Although it is not possible to assess quantitatively the relative heights of the energy levels or the widths of any bands formed, qualitatively, at least three factors must be considered. These factors, which all change with and depend on the particular metal ion forming the compound, are as follows.

The Height of the Energy Levels of the Cation with Respect to the Anion.—The closer these levels are to each other before any mixing takes place, the stronger they will interact on mixing. It is known that the d-electron levels of the transition metals decrease in energy (increase in stability) with increasing number of d electrons, as a result of imperfect d-electron shielding. Each additional electron thus sees a larger effective nuclear charge which slightly reduces its spatial extension and increases its ionization potential. This means that, as the number of d electrons increases in the transition metal series, the tendency toward covalent rather than ionic bond formation increases. Therefore, in considering ionization potentials alone, bands formed from covalent anion–cation interaction will tend to broaden in going from MnS_2 to CuS_2, being abnormally wide for CuS_2. In addition, Δ_{cov} should also increase in the same manner, being largest for CuS_2.

The Number of Antibonding Electrons.—When an electron is added to an antibonding level, the system suffers an energy loss with respect to the total energy before this electron was added. Therefore, the population of antibonding levels will result in a decrease in the cohesive bonding forces in the crystal. This will manifest itself in increasing interatomic distances, larger unit cells, and ultimately a decrease in width of the e_g band.

Exchange Energies.—If the amount of energy gained by intraatomic stabilization is large (as in the case of five unpaired electrons on the same ion), band width should decrease since decreasing covalent interaction will allow electrons to be more localized on the cation. Exchange considerations should be important only for high-spin Mn^{2+} and possibly Ni^{2+}, where there can be five and two unpaired electrons, respectively. None of the other ions in this series can have more than one unpaired electron when in the low-spin state.

It is thus apparent from the foregoing considerations that several competing factors will influence covalent interaction, band width, and interatomic distances. Recourse to transport properties and optical data is one way to assess the relative contributions of each factor. With these considerations in mind, it is appropriate first to consider energy level diagrams that correspond to the actual compounds. This will be followed by a discussion of their optical properties.

MnS_2.—Intraatomic exchange stablization will be a maximum in the 3d series for Mn^{2+} since the cation has five unpaired electrons in the high-spin state. Therefore, it has the maximum tendency to localize the electrons, resulting in very narrow bands. This exchange energy has the effect of splitting the d levels into spin-up and spin-down states separated by Δ_{ex} (Figure 9).

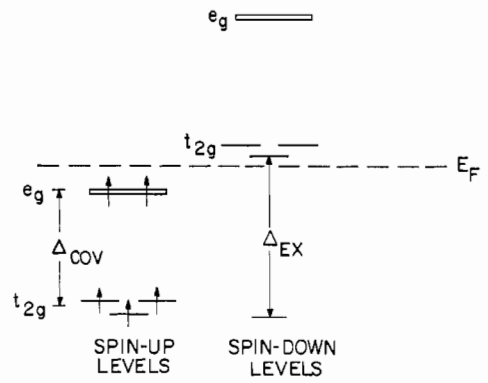

Figure 9.—Schematic energy level diagram for MnS_2 d levels. Intraatomic exchange can be represented as a splitting of the 10 d states into 5 spin-up and 5 spin-down levels. E_F denotes that energy below which the last electron has been added.

A temperature-dependent Curie–Weiss susceptibility corresponding to the full five unpaired electrons is expected above T_N or T_C. All occupied spin-up levels are filled, so semiconductor properties are anticipated.

The activation energy would correspond to a $^6S \rightarrow {}^4T_{1g}$ spectral transition for an Mn^{2+} ion[36] which would leave a hole in the e_g band. If the e_g bands in MnS_2 are so narrow that they can be considered as localized levels, then the activation energy for conduction would correspond to a transition from the d to the sp levels as in ZnS_2. The cell size should reflect the ionic character and MnS_2 does have the largest unit cell (6.109 Å) of the MS_2 compounds. The magnetic properties of MnS_2[27] indicate five unpaired electrons. Although electrical data have not been reported for MnS_2, $MnSe_2$ has an energy gap of 0.2 eV.[16]

FeS_2.—Semiconductor properties are anticipated with an activation energy corresponding to an electron transfer from the filled t_{2g} level to the empty σ^* band (Figure 10). Iron disulfide should also be diamagnetic with a relatively high negative Seebeck coefficient. These considerations are consistent with the data of Table II.

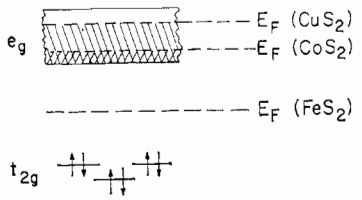

Figure 10.—Energy level diagrams for FeS_2, CoS_2, and CuS_2.

Since there are no antibonding electrons in FeS_2, the e_g band should be broad. The observed high electron mobility of 230 cm^2/V sec confirms this supposition. In this connection, it is of interest to examine published mobility data[31] on mineral samples where both p- and n-type conductivity were observed. It seems logical to assume that the p-type samples contain acceptor centers above the filled t_{2g} levels while the n-type samples contain donor centers below the empty e_g band. For all samples measured, hole mobility was much lower than electron mobility, suggesting that the t_{2g} levels are very nearly localized relative to the e_g levels. This also implies that it is correct to consider the t_{2g} levels of the metal ion as separate from the broad σ-bonding band, since an overlapping σ band would lead to a high p-type mobility. The absence of antibonding electrons should lead to the shortest anion–cation distance and the smallest unit cell, as is observed (5.4182 Å).

It should be noted that to be consistent with experimental data, it is necessary to assume that the covalent interaction is strong enough to result in $\Delta_{cov} > \Delta_{ex}$ for Fe^{2+}. It seems likely, therefore, that in the pyrite sulfides $\Delta_{cov} < \Delta_{ex}$ only for Mn^{2+}, in which there can be five unpaired electrons.

CoS_2.—Cobalt disulfide should be an n-type, metallic conductor because of the quarter-filled σ^* band (Figure 10). Occupancy of the antibonding band should result in an effective shrinking of the band width. Therefore, it is possible for this compound to be metallic and still exhibit a paramagnetic moment at high temperatures because of this narrow band width. This means that Pauli paramagnetism, characteristic of broad-band metals, will not be observed. The data of Table II are consistent with these considerations.

If some indirect interaction is favored at low temperatures, it is expected to be weak (low T_N or T_C) since no strong internal field is present; *i.e.*, no localized, unpaired t_{2g} electrons with which the metallic electrons can correlate. The observed ferromagnetism (T_C = 118°K) is consistent with the electronic phase diagram of Goodenough,[37] which predicts a ferromagnetic moment of $\leq n_d \mu_B$ for a sufficiently narrow quarter-filled band (n_d for CoS_2 would be the number of electrons in the e_g band).

NiS_2.—In NiS_2 it is assumed that intraatomic exchange is greater than the band width and therefore will split the energy levels into spin-up and spin-down states (Figure 11). This would require that NiS_2 be a

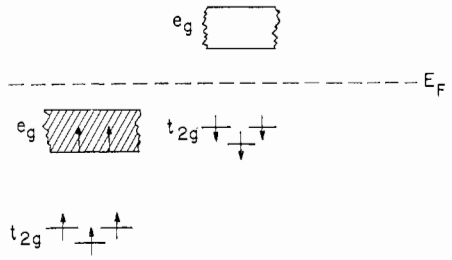

Figure 11.—Energy level diagram for NiS_2. The filled lower e_g band is considered to be narrow enough for the electrons to be polarized in a spin-up direction.

semiconductor with an activation energy corresponding to that required to transfer an electron from the filled spin-up band to the empty spin-down band. Figure 11 does not imply a ferromagnetic moment corresponding to two unpaired electrons. The band gap is the difference between the unpaired and the paired spin state. If this difference is less than the band width (as is believed to be the case for $NiSe_2$) the spin-paired state will be obtained and will show either weak temperature-independent paramagnetism or diamagnetism. If the band gap is larger than the band width, as in NiS_2, a paramagnetic Curie–Weiss state will exist with two unpaired spins per nickel ion.[38] Some type of ordered magnetic state will exist at low temperatures. The magnetic structure will be determined by the relative signs and magnitudes of nearest neighbor and next nearest neighbor exchange integrals. In order to avoid the problem of translational symmetry on an antiferromagnetic sublattice (it is impossible to propagate strong antiferromagnetic coupling in an fcc lattice using only nearest neighbor interactions), Figure 11 should be considered as schematically representing a particular Ni ion with the direction of the resultant unpaired electrons alternating from one Ni ion to another in a peri-

(36) L. E. Orgel, "An Introduction to Transition Metal Chemistry," Methuen and Co., Ltd., London, 1960, p 90.

(37) J. B. Goodenough, *J. Appl. Phys.*, **38**, 1054 (1967).

(38) H. S. Jarrett, W. H. Cloud, R. J. Bouchard, C. G. Frederick, S. R. Butler, and J. L. Gillson, *Phys. Rev. Letters*, **21**, 617 (1968). This work shows that in the $Co_{1-x}Ni_xS_2$ system the nickel contributes a moment of two unpaired spins to the paramagnetic moment (μ_{eff}^2). At low temperature this moment is aligned antiparallel to the one unpaired electron associated with the cobalt atom.

odicity as yet undetermined. On the basis of this qualitative model, several possible mechanisms could lead to metallic conductivity in the presence of small deviations from stoichiometry, *e.g.*, holes in the spin-up band or electrons in the spin-down band.

If, as the chemical analysis suggests, the low-pressure, semiconducting form is sulfur deficient, electrons are introduced into the spin-down band. These must be very immobile because the material acts like an intrinsic semiconductor in which the holes have a higher mobility than the electrons. On the other hand, the high-pressure, sulfur-excess material should act like a degenerate, p-type semiconductor as is observed. As mentioned earlier, the low-temperature, weak ferromagnetism can be accounted for if one assumes that the extra electrons in sulfur-deficient NiS_2 are localized, perhaps at a sulfur vacancy.

CuS_2.—Copper disulfide should be a p-type metallic conductor because of the three-quarters-filled band (Figure 10). In CuS_2, the e_g levels are closest to those of the anion and can, therefore, mix most effectively of all the transition metal ions. Metallic conductivity and a small positive Seebeck voltage (Table I) are in agreement with a model in which the three e_g electrons are in a single antibonding band. These properties result in Pauli paramagnetism.

The fact that the structure of CuS_2 is cubic furnishes additional evidence that a band model is more appropriate than an ionic one. If these were ionic materials, a pyrite containing Cu^{2+} would be expected to exhibit a Jahn–Teller distortion from cubic symmetry. (One would also expect a J–T distortion for low-spin CoS_2 if its one e_g electron were localized.)

ZnS_2.—The d states are filled so no σ or σ_* bands of any width will be formed since filled anion orbitals cannot mix effectively with filled metal orbitals. In any case, a localized-electron model and a band model containing only filled bands are equivalent. Zinc disulfide should, therefore, be a diamagnetic semiconductor with an activation energy corresponding to the transfer of an electron from the highest e_g level to the broad s–p band (Table I). It is also possible in ZnS_2 that the d levels may be below the top of the broad σ band. In this case the lowest energy electron transfer would be between an admixed band comprised of e_g, t_{2g}, and σ-anion states and the upper s–p antibonding band.

Optical Properties.—The foregoing considerations are consistent with the following interpretation of the optical properties. In FeS_2, the t_{2g} levels are filled and the e_g (σ^*) band is empty. The absorption edge of the lowest energy peak, E_1 (Figure 2), therefore corresponds to the onset of t_{2g}–e_g transitions. The energy of this optical band gap (0.9 ± 0.1 eV) agrees with the observed activation energy of electrical conduction (0.46 eV = $E_a \equiv \Delta E/2$). The next available level to which excitation can take place is the antibonding s–p band. From the yellow color of ZnS_2, it can be concluded that this band is at least 2.5 eV above the d levels. Neglecting the width of the e_g band, the energy of t_{2g}–sp transitions must therefore be at least 2.5 eV in FeS_2. This leads to the conclusion that the E_2, E_3, and E_4 absorption peaks are probably also due to t_{2g}–e_g transitions.

It is possible that some of the absorption peaks on the high-energy side of the major peaks may be due to valence band (σ) → e_g transitions. Since the energy separation between the cation and anion levels is not known, this possibility cannot be excluded. The drop in absorption after the main peak, however, suggests that the valence band is not contributing at low energies since an absorption continuum would be expected if this were so. The major point to be derived from the previously mentioned energy considerations is that, regardless of the origin of the electrons in the optical transitions, the low-energy optical bands must represent transitions terminating at the e_g band and not the higher s–p band.

For the remainder of the discussion, only the E_2 band of each compound will be considered since the other peaks represent fine structure of this principal absorption band. The absorption bands of FeS_2, CoS_2, and NiS_2 are similar in structure, indicating that the same transition is responsible for the observed spectra in all of the compounds in Figure 2 at energies below 3 eV. With increasing atomic weight of the cation, a shift of the bands to lower energies is observed. This may be related to a steady decrease in Δ_{cov}.

Alternatively, as pointed out by Goodenough,[39] the t_{2g} levels of the cation may be gradually falling below the top of the broad, filled, bonding band as the stability of the d levels increases (energy decreases) from Fe to Zn. This would be reflected in an apparent decrease in Δ_{cov}, but then Δ_{cov} would no longer retain its original significance, since the onset of the measured optical transition would represent the energy separation between the top of the broad σ band (admixed with the t_{2g} states) and the e_g band. This explanation is actually more consistent with the increased Δ_{cov} expected with increasing atomic number, a factor mentioned previously.

In order to compare the degree of covalent mixing in the e_g band of these compounds, it is convenient to discuss the oscillator strengths, f. This quantity increases with increasing degree of covalent mixing (increasing sp character) in the e_g band. Instead of the actual oscillator strengths, f sums have been calculated for use in this comparison. In Figures 3 and 4, n_{eff} is plotted for these compounds as a function of energy where

$$Nn_{eff} = \frac{1}{\hbar}\int_0^{E_0} f(E)\mathrm{d}E = \frac{m}{2\pi^2 e^2}\int_0^{\omega_0} \omega \mathrm{Im}\tilde{\epsilon}(\omega)\ \mathrm{d}\omega$$

and N is the number of molecules per unit volume.[7] The f sum rule states that $\lim_{E\to\infty} n_{eff} = n$, where n is the total number of electrons per molecule.[7] If the energy separation between adjacent bands is very large, the absorption spectrum of valence electrons may be nearly complete before absorption by core electrons becomes possible at higher energy. In such a case, a plot of n_{eff} *vs.* energy would show distinct steps.[40] For the

(39) J. B. Goodenough, personal communication.
(40) H. R. Philipp and H. Ehrenreich, *Phys. Rev.*, **129**, 1550 (1963).

pyrites, however, adjacent bands are close together in energy and the presence of conduction electrons further decreases the sharpness of the boundaries between different absorption regions. Nevertheless, some information can be obtained from a comparison of the slopes of the n_{eff} curves of the CuX_2 compounds which have similar electronic structures (Figure 3). Since the band filling is identical in all of the copper compounds, *i.e.*, six t_{2g} and three e_g conduction electrons per CuX_2 unit, the increase in the slope of n_{eff} *vs.* energy in the series S → Se → Te can be attributed to an increase in the oscillator strength of the t_{2g}–e_g transitions, *i.e.*, increased covalency. At lower energies (<0.5 eV), the n_{eff} curves are expected to contain contributions from intraband conduction electrons. At higher energies, contributions from transitions to sp levels will become increasingly important. Even with these restrictions, it may be concluded that the amount of covalent mixing in the e_g band increases as expected when the anion becomes more polarizable.

A direct comparison of the n_{eff} curves of FeS_2, CoS_2, NiS_2, and CuS_2 (Figure 4) is complicated by the fact that a different number of e_g electrons is present in each compound. The number of empty states in the e_g band to which a t_{2g}–e_g transition is possible thus changes from one compound to the next. Even if f remains constant, n_{eff} at the high-energy side (2.5 eV is a reasonable estimate) of the t_{2g}-e_g absorption band should be proportional to the number of available states in the e_g band, *i.e.*, in the ratio $4(FeS_2):3(CoS_2):2(NiS_2):1(CuS_2)$. After subtracting 0.3 from the observed n_{eff} values of CoS_2 and CuS_2 to correct for the intraband transitions by conduction electrons, the following n_{eff} ratios are found (Figure 4) at 2.5 eV: $FeS_2:CoS_2:NiS_2:CuS_2 = 1.18:0.88:0.51:0.30 = 4.0:3.0:1.7:1.0$. The fact that the n_{eff} ratios closely mirror the statistical transition probability suggests that the degree of covalent mixing, as measured by the oscillator strengths, is not very different for the four compounds.

It is interesting to note that FeS_2 and Si have approximately the same band gap and energy dependence of n_{eff}.[40] Since the conduction band in Si is approximately 10 eV wide[41] as compared to an estimated 1–1.5 eV in FeS_2, the oscillator strength is considerably less in the latter. The next band at higher energy for FeS_2 (sp band) contributes more to n_{eff} than does the e_g band. As shown (Figure 4), $n_{eff} \simeq 3$ at 5 eV, the limit of the measurements. Since a maximum of $n_{eff} = 6$ would be expected if all valence electrons were absorbing, it is concluded that a major part of the total absorption spectrum has been observed. This is also shown by the plot of

$$\epsilon_{0,eff}(\omega_0) = 1 + \frac{2}{\pi}\int_0^{\omega_0} \omega^{-1}\mathrm{Im}\tilde{\epsilon}(\omega)\, d\omega$$

vs. energy (Figure 4). According to the Kramers–Kronig relations[7]

$$\epsilon_0 = \lim_{\omega_0 \to \infty} \epsilon_{0,eff}(\omega_0)$$

where ϵ_0 is the static dielectric constant. Gillson[42] found from interference patterns observed in transmission spectra of FeS_2 that ϵ_0 is 24 in the range 0.15–5 eV. Figure 4 shows that at 5 eV, $\epsilon_{0,eff} = 19.6$ confirming the assumption that a major part of the total FeS_2 absorption spectrum has been observed.

Summary

An empirical model depicting the qualitative band structure of the first-row transition metal, pyrite-type dichalcogenides has been presented that emphasizes covalent cation–anion interactions. This model is consistent with electrical, magnetic, and optical measurements and explains the progressive increase in cell size in going from FeS_2 to ZnS_2 as the result of the addition of antibonding electrons. The largest numbers of antibonding electrons are present in CuS_2 and ZnS_2, indicating that they should be the least stable compounds and the most difficult to prepare. This accords with the experimental fact that only CuS_2 and ZnS_2 require high pressure for their syntheses.

While this discussion has been primarily limited to the MS_2 pyrites, it can be logically extended to the selenides and tellurides. When selenium or tellurium is substituted for sulfur, the bands resulting from covalent interaction must broaden because of the higher polarizability of these two chalcogenides. Therefore, the properties will reflect an increased tendency toward delocalization of the e_g electrons with corresponding higher mobilities and lower activation energies for conduction. Interpretation will become less clear when the anion is tellurium since the d levels may no longer be separated in energy from the anion levels, especially when the metal levels are very stable, as in $CuTe_2$.

Acknowledgments.—We wish to thank C. L. Hoover and A. W. Larchar for supervision of the high-pressure experiments, P. E. Bierstedt and J. L. Gillson for Meissner and resistivity measurements, R. B. Flippen and J. F. Weiher for magnetic susceptibility data, J. R. Barkley for suggesting use of the computer search program for the analysis of the optical measurements, M. T. Jones for Mössbauer measurements on the iron dichalcogenides, the members of the Central Research Department X-ray group for diffraction data, and H. S. Jarrett and H. S. Young for many helpful discussions pertaining to this work. In addition, we wish to express our sincere appreciation to J. B. Goodenough of Lincoln Laboratory, Massachusetts Institute of Technology, Lexington, Mass., for many helpful comments pertaining to the model discussed herein.

(41) J. Calloway, *Solid State Phys.*, **7**, 99 (1958).

(42) J. L. Gillson, private communication.